New Adducts of Dirhodium(II) Formamidinate Complexes with Polycyano Acceptor Molecules. X-ray Crystal Structure of the Tricyanomethanide Complex $Rh_2(form)_4[C(CN)_3]$ (form = *N*,*N*′-Di-*p*-tolylformamidinate)

Sandra Lo Schiavo,[†] Giuseppe Bruno,[†] Piero Zanello,[‡] Franco Laschi,[‡] and Pasquale Piraino*,[†]

Dipartimento di Chimica Inorganica, Analitica e Struttura Molecolare, Università di Messina, Messina, Italy, and Dipartimento di Chimica, Università Siena, Siena, Italy

Received April 9, 1996[⊗]

The dirhodium(II) formamidinate complexes $Rh_2(form)_2(O_2CCF_3)_2(H_2O)_2$ (**I**) and $Rh_2(form)_4$ (**II**, form = *N*,*N*′-di-*p*-tolylformamidinate) react with the polycyano acceptor molecules tetracyanoethylene (TCNE), tetracyano-*p*-quinodimethane (TCNQ), 2,5-dimethyl-*N*,*N*′-dicyano-*p*-quinonediimine (2,5-DMDCNQI), and *N*,*N*′-naphthocyano-*p*-quinonediimine (NCNQI) giving species whose nature is critically dependent on the redox potentials of the two parent complexes. Complex **I** reacts *via* axial coordination with negligible charge transfer (CT) from the dimetal unit to the ligand. With TCNE, it gives the labile monoaxial adduct $Rh_2(form)_2(O_2CCF_3)_2$(TCNE) (**1**), which easily loses the cyano ligand restoring the parent complex. TCNQ, 2,5-DMDCNQI, and NCNQI react with **I** giving polymeric materials of composition $\{[Rh_2(form)_2(O_2CCF_3)_2]_2TCNQ)\}_n$ (**2**) and $[Rh_2(form)_2(O_2CCF_3)_2X]_n$ (X = 2,5-DMDCNQI (**3**), NCNQI (**4**)). The reaction of **II** with TCNE, TCNQ, and 2,5-DMDCNQI proceeds *via* a single electron transfer from the dimetal unit to the cyano ligand to form the CT species $[Rh_2(form)_4X]$ (X = TCNE (**5**), TCNQ (**6**), 2,5-DMDCNQI (**7**)). Electrochemical and EPR measurements suggest a different extent of coordination between the polycyano fragment and the dirhodium unit, depending upon the polarity of the solvents. Attempts to crystallize complex **5** from acetonitrile unexpectedly led to the formation of the tricyanomethanide complex $Rh_2(form)_4[C(CN)_3]$ (**5A**), arising from the unprecedented transformation of the tetracyanoethylenide ion into the tricyanomethanide anion. The complex crystallizes in the tetragonal *P*4/*ncc* space group with $a = 14.169(6)$ Å, $c = 29.20(2)$ Å, $V = 5863(5)$ Å^3, and $Z = 4$. The molecule consists of a dirhodium unit symmetrically bridged by four formamidinate ligands and one tricyanomethanide anion N-coordinated at the axial position of Rh(2).

Introduction

Redox-active transition metal complexes are of increasing interest since they may be involved in intermolecular electron transfer processes, which are fundamental phenomena occurring as primary events in several chemical reactions. Furthermore, they may provide a good entry to charge-transfer based materials incorporating transition metal complexes as donor or acceptor species.

Some years ago, we reported the synthesis[1] and PE spectra[2] of the complexes $Rh_2(form)_2(O_2CCF_3)_2(H_2O)_2$ (**I**) and $Rh_2(form)_4$ (**II**) (form = *N*,*N*′-di-*p*-tolylformamidinate). The PE spectra evidenced progressive destabilization of all valence shells on going from $Rh_2(form)_2(O_2CCF_3)_2(H_2O)_2$ to $Rh_2(form)_4$. In accordance with these findings, electrochemical investigations[1−3] evidenced that the progressive substitution of oxygen atoms in the coordination sphere of the complex $Rh_2(O_2CCF_3)_4$ with nitrogen atoms causes dramatic effects on the redox properties of the resulting complexes. The four- and eight-nitrogen coordination favors the thermodynamic stabilization of mixed-valent species containing the Rh_2^{5+} core, as a consequence of the increased electron richness of the complexes. Accordingly, we obtained the cation radical species $[Rh_2(form)_2(O_2CCF_3)_2]^{\bullet+}$ and $[Rh_2(form)_4]^{\bullet+}$ as very stable compounds.[4] Furthermore, the X-ray analysis of the neutral and mono-oxidized species reveals that no significant structural distorsions are involved in the course of the electron-transfer step, so that the electron-transfer processes are favored by the small reorganization barriers. Therefore, the species $Rh_2(form)_2(O_2CCF_3)_2(H_2O)_2$ and $Rh_2(form)_4$ appear as suitable substrates for electron-transfer reactions with accepting molecules.

This paper focuses on the electron-transfer reactions between the above-named complexes and the polycyano acceptor molecules tetracyanoethylene, tetracyano-*p*-quinodimethane, 2,5-dimethyl-*N*,*N*′-dicyano-*p*-quinonediimine, and *N*,*N*′-naphthocyano-*p*-quinonediimine, which were recognized to form conducting charge transfer (CT) complexes as well as highly conducting salts.[5] We report also the X-ray analysis of the complex $Rh_2(form)_4[C(CN)_3]$ arising from the unprecedented transformation of a $TCNE^{\bullet-}$ anion radical into the $[C(CN)_3]^-$ anion.

Experimental Section

All the reactions were initially performed in a dry nitrogen atmosphere, and the solvents were distilled by standard techniques and deoxygenated before use. However, by that time we noticed that the

[†] Università di Messina.
[‡] Università di Siena.
[⊗] Abstract published in *Advance ACS Abstracts,* January 15, 1997.

(1) (a) Piraino, P.; Bruno, G.; Tresoldi, G.; Lo Schiavo, S.; Zanello, P. *Inorg. Chem.* **1987**, *26*, 91. (b) Piraino, P.; Bruno, G.; Lo Schiavo, S.; Laschi, F.; Zanello, P. *Inorg. Chem.* **1987**, *26*, 2205.
(2) Rizzi, G. A.; Casarin, M.; Tondello, E.; Piraino, P.; Granozzi, G. *Inorg. Chem.* **1987**, *26*, 3406.
(3) Chavan, M. Y.; Zhu, T. P.; Lin, X. Q.; Ahsan, M. Q.; Bear, J. L.; Kadish, K. M. *Inorg. Chem.* **1984**, *23*, 4538.
(4) (a) Bruno, G.; Tresoldi, G.; Lo Schiavo, S.; Sergi, S.; Piraino, P. *Inorg. Chim. Acta* **1992**, *197*, 9. (b) Bruno, G.; Lo Schiavo, S.; Tresoldi, G.; Piraino, P.; Valli, L. *Inorg. Chim. Acta* **1992**, *196*, 131.
(5) (a) Hunig, S.; Erk, P. *Adv. Mater.* **1991**, *3*, 225. (b) Endres, H. *Extended Linear Chains Compounds*; Miller, J. S., Ed; Plenum Press: New York, 1993; Vol. 3, p 263.

S0020-1669(96)00386-2 CCC: $14.00

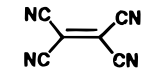

TCNE

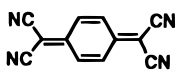

TCNQ

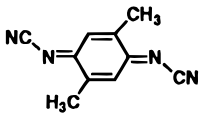

2,5-DMDCNQI

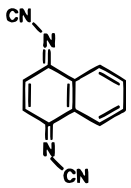

NCNQI

use of aerobic conditions does not alter the course of the reaction. TCNE (tetracyanoethylene) and TCNQ (tetracyano-*p*-quinodimethane) were used as supplied from Aldrich Chemicals. $Rh_2(form)_4$,[1b] $Rh_2(form)_2(O_2CCF_3)_2(H_2O)_2$,[1a] 2,5-DMDCNQI (2,5-dimethyl-*N*,*N*′-dicyano-*p*-quinonediimine),[6] NCNQI (*N*,*N*′-naphthocyano-*p*-quinonediimine),[6] and $K[C(CN)_3]$[7] were synthesized according to literature reports. Infrared spectra were recorded on a Perkin-Elmer FT 1720 X spectrometer, while UV−vis-near-IR spectra were recorded on a Perkin-Elmer Lambda 2 spectrometer. The apparatus for the electrochemical and EPR measurements have been described elsewhere.[8] Anhydrous acetonitrile, tetrahydrofuran, and dichloromethane solvents were Aldrich products, packaged under nitrogen in 100 mL bottles. Tetraethylammonium perchlorate and tetrabutylammonium hexafluorophosphate, electrochemical grade, were Fluka products. Potential values are referenced to the saturated calomel electrode (SCE). Under the present experimental conditions, the one-electron oxidation of ferrocene occurs at $E^{\circ\prime} = +0.38$ V in MeCN, at $E^{\circ\prime} = +0.39$ V in CH_2Cl_2, and at $E^{\circ\prime} = +0.52$ V in THF solution.

Synthesis of $[Rh_2(form)_2(O_2CCF_3)_2TCNE]$ (1). To a stirred benzene solution of $Rh_2(form)_2(O_2CCF_3)_2(H_2O)_2$ (0.1 g, 0.1 mmol) was added crude TCNE (0.013 g, 0.1 mmol). The original green-yellow solution immediately turns dark green while a precipitate slowly forms. After 3 h, the precipitate was separated from the colorless solution and washed with benzene. Yield: 96%. Anal. Calcd for $Rh_2C_{40}H_{30}N_8O_4F_6$: C, 47.73; H, 3.00; N, 11.13. Found: C, 47.89; H, 3.1; N, 11.4. Infrared spectrum (Nujol mull, cm^{-1}): ν(CN) 2237 (s), 2202 (s).

Synthesis of $\{[Rh_2(form)_2(O_2CCF_3)_2]_2TCNQ\}_n$ (2). The synthesis of **2** was identical with that of **1** except that 0.1 g (0.1 mmol) of $Rh_2(form)_2(O_2CCF_3)_2(H_2O)_2$ and 0.01 g (0.05 mmol) of TCNQ were used to yield a red-brown precipitate. Yield: 90%. Anal. Calcd for $Rh_2C_{80}H_{64}N_{12}O_8F_{12}$: C, 49.00; H, 3.28; N, 8.57; F, 11.62. Found: C, 49.28; H, 3.3; N, 8.64; F, 11.82. Infrared spectrum (Nujol mull, cm^{-1}): ν(CN) 2215 (s).

Synthesis of $[Rh_2(form)_2(O_2CCF_3)_2(2,5\text{-}DMDCNQI)]_n$ (3). This complex was prepared by adding 2,5-DMDCNQI (0.018 g, 0.1 mmol) dissolved in benzene to 0.1 g (0.1 mmol) of **I.** An immediate reaction takes place with the formation of a black-green precipitate, which was collected, washed several times with benzene, and dried. Yields 95%. Anal. Calcd for $Rh_2C_{44}H_{38}N_8F_6O_4$: C, 49.73; H, 3.6; N, 10.54; F, 10.72. Found: C, 50.1; H, 3.65; N, 10.58; F, 10.55.

Synthesis of $[Rh_2(form)_2(O_2CCF_3)_2(NCNQI)]_n$ (4). This complex was prepared as before forming a dark compound. Yield: 95%. Anal. Calcd for $Rh_2C_{46}H_{36}N_8O_4F_6$: C, 50.94; H, 3.34; N, 10.33; F, 10.50. Found: C, 51.0; H, 3.4; N, 10.54; F, 10.65.

Synthesis of $[Rh_2(form)_4TCNE]$ (5). Complex **5** was synthesized by reacting 0.1 g (0.091 mmol) of $Rh_2(form)_4$ dissolved in benzene with 0.012 g (0.093 mmol) of solid TCNE. The red mixture was stirred for 1 h during which time a pink-red precipitate slowly formed. After filtration, the solid was washed several times with benzene. Yield: 84%. Anal. Calcd for $Rh_2C_{66}H_{60}N_{12}$: C, 64.60; H, 4.92; N, 13.69. Found: C, 64.5; H, 5.0; N, 13.5. Infrared spectrum (Nujol mull, cm^{-1}): ν(CN) 2198 (s), 2154 (vs). Electronic spectrum (CH_3CN, λ_{max}, nm ($\epsilon \times 10^3$, M^{-1} cm^{-1})): 428 (8.4), 910 (5.78). Molar conductivity (Ω^{-1} cm^2 M^{-1}): λ 140 (CH_3CN, 10^{-4} M).

Synthesis of $[Rh_2(form)TCNQ]$ (6). Operating as before, a black solid was obtained. Yield: 90%. Anal. Calcd for $Rh_2N_{12}C_{72}H_{64}$: C, 66.35; H, 4.95; N, 12.79. Found: C, 65.95; H, 5.0; N, 12.65. Infrared spectrum (Nujol mull, cm^{-1}): ν(CN) 2193 (vs), 2163(s). Electronic spectrum (CH_3CN, λ_{max}, nm ($\epsilon \times 10^4$, M^{-1} cm^{-1})): 842 (4.34), 420 (2.44). Molar conductivity (Ω^{-1} cm^2 M^{-1}): λ 125 (CH_3CN, 10^{-4} M).

Synthesis of $[Rh_2(form)_4(2,5\text{-}DMDCNQI)]$ (7). To a benzene solution of $Rh_2(form)_4$ (0.1 g, 0,09 mmol) was added 0.016 g (0.09 mmol) of solid 2,5-DMDCNQI. The reaction mixture immediately changes from light green to blue. After 2 h, the reaction mixture was concentrated in vacuo, and then *n*-heptane was added inducing the precipitation of a blue solid. Yield: 87%. Anal. Calcd for $Rh_2N_{12}C_{70}H_{68}$: C, 65.52; H, 5.34; N, 13.09. Found: C, 65.7; H, 5.5; N, 12.95. Infrared spectrum (Nujol mull, cm^{-1}): ν(CN) 2134 (s), 2161(w). Electronic spectrum (acetone, λ_{max}, nm (ϵ x 10^4, M^{-1} cm^{-1})): 628 (2), 696 (1.83), 933 (0.58). Molar conductivity (Ω^{-1} cm^2 M^{-1}): λ 55 (CH_3CN, 10^{-4} M).

Synthesis of $Rh_2(form)_4[C(CN)_3]$ (5A). Complex **5** (0.3 g, 0.24 mmol) was dissolved in 50 mL of CH_3CN, and the solution was allowed to stand for 7 days at room temperature. During this time, slow evaporation of the solvent occurred, leaving a crop of red crystals which were collected and dried. Yield: 54%. Anal. Calcd for $Rh_2C_{64}H_{60}N_{11}$: C, 64.64; H, 5.08; N, 12.95. Found: C, 64.5; H, 5.18; N, 12.63. Infrared spectrum (Nujol mull, cm^{-1}): ν(CN) 2220 (w), 2180 (s). Electronic spectrum (CH_3CN, λ_{max}, nm ($\epsilon \times 10^3$, M^{-1} cm^{-1})): 426 (5.2), 513 (5.25), 916 (5.86). Molar conductivity (Ω^{-1} cm^2 M^{-1}): λ 120 (CH_3CN, 10^{-4} M).

Table 1. Crystallographic Data for $Rh_2(form)_4[C(CN)_3]$

formula	$C_{64}H_{60}N_{11}Rh_2$
fw	1189.05
space group	*P*4/*ncc* (No. 130)[13]
a, Å	14.169(6)
c, Å	29.20(2)
V, Å^3	5863(5)
Z	4
ρ_{calcd}, g/cm^3	1.347
μ (Mo Kα), mm^{-1}	0.612
λ (graphite monochromated), Å	0.710 73 (Mo Kα)
T, K	293
R^a (refined/all)	0.054/0.256
$R_w{}^b$ (refined/all), on F^2	0.079/0.106

^{a} $R = [\Sigma|F_o| - |F_c|]/\Sigma|F_o|$. ^{b} $R_w = [\Sigma w(F_o^2 - F_c^2)^2/\Sigma_w(F_o^2)^2]^{1/2}$.

X-ray Data Collection and Structure Refinement. Suitable crystals of **5A** were obtained by slow evaporation (7 days) of solvent from an acetonitrile solution of complex **5**. A summary of the crystallographic data and the structure refinements is listed in Table 1, while details are given in Table S1 of the Supporting Information. Diffraction data were collected at room temperature on a Siemens R3m/V automatic four-circle diffractometer using graphite-monochromated Mo Kα radiation. The reflection intensities were evaluated by a profile-fitting among 2θ shells procedure[9] and then corrected for Lorentz-polarization effects. An absorption correction was applied by fitting a pseudo-ellipsoid to the azimuthal scan data of 12 high-χ reflections ($R_{int} = 1.99\%$).[10] The systematic absences indicated uniquely the space group *P*4/*ncc* of the tetragonal system.

The structure was solved by standard Patterson methods by using the SHELXTL-PLUS system[11] (used to perform data reduction also).

(6) Aumuller, A.; Hunig, S. *Liebigs Ann. Chem.* **1986**, 142.
(7) Trofimenko, S.; Little, E. L.; Mower, H. F. *J. Org. Chem.* **1962**, *27*, 433.
(8) (a) Bianchini, C.; Laschi, F.; Masi, D.; Ottaviani, F. M.; Pastor, A.; Peruzzini, M.; Zanello, P.; Zanobini, F. *J. Am. Chem. Soc.* **1993**, *115*, 2723. (b) Zanello, P.; Bartocci, C.; Maldotti, A.; Traverso, O. *Polyhedron* **1983**, *2*, 791.
(9) Diamond, R. *Acta Crystallogr., Sect. A* **1969**, *25*, 43.
(10) Kopfmann, G.; Huber, R. *Acta Crystallogr., Sect. A* **1968**, *24*, 348.
(11) Sheldrick, G. M. *SHELXTL-PLUS*, Version 4.2; Siemens Analytical X-ray Instruments, Inc.: Madison, Wisconsin, 1991.

Table 2. Atomic Coordinates ($\times 10^4$) and Equivalent Isotropic Displacement Coefficients ($Å^2 \times 10^3$) for $Rh_2(form)_4[C(CN)_3]$

atom	x	y	z	U_{iso}/U_{eq}[a]
Rh(1)	2500	2500	1599(1)	85(1)[a]
Rh(2)	2500	2500	2442(1)	76(1)[a]
C(1)	799(9)	3626(8)	1266(4)	97(8)
C(2)	1098(7)	3618(8)	813(5)	129(8)
C(3)	450(11)	3754(8)	461(3)	126(8)
C(4)	−497(9)	3897(9)	564(4)	112(8)
C(5)	−796(6)	3905(8)	1017(5)	115(9)
C(6)	−148(10)	3770(7)	1368(3)	82(7)
C(7)	1712(8)	4428(8)	2756(3)	74(6)
C(8)	2130(6)	5308(9)	2704(3)	102(7)
C(9)	2055(7)	5978(7)	3050(4)	109(8)
C(10)	1560(8)	5766(8)	3448(3)	87(7)
C(11)	1141(6)	4886(9)	3500(3)	93(7)
C(12)	1217(7)	4217(6)	3154(4)	85(7)
C(13)	−1210(15)	4037(16)	190(6)	212(16)[a]
C(14)	1462(13)	6455(13)	3830(6)	142(9)[a]
C(15)	1357(11)	3982(12)	2005(6)	80(6)
N(1)	1449(14)	3474(14)	1629(4)	88(5)
N(2)	1778(9)	3736(9)	2393(4)	69(5)
N(3)	2500	2500	3151(9)	98(12)
C(16)	2500	2500	3528(12)	91(13)
C(17)	2500	2500	4061(16)	114(15)
C(18)	1721(35)	2938(47)	4313(16)	267(43)
N(4)	980(30)	2708(39)	4395(16)	250(24)

[a] Equivalent isotropic U defined as one third of the trace of the orthogonalized $\mathbf{U}_{ij}$ tensor.

Then, the refinement of the model was continued with SHELXL-93.[12] Serious problems in the refinement cycles come from the disorder of the tricyanomethanide anion (TCM), due to its position on the crystallographic 4-fold axis of symmetry passing through its central carbon atom and one CN group. In fact, the symmetry operator generates four positions of the other CN fragment that must be treated as two possible orthogonal orientations (each one with 50% occupancy) of the TCM ligand. Neutral-atom scattering factors and anomalous dispersion corrections are from ref 13.

Final geometrical calculations and drawings were carried out with the PARST program[14] and the XP utility of the Siemens package, respectively. Final fractional coordinates are reported in Table 2, while selected bond distances and angles are listed in Table 3. An ORTEP view of the molecular structure of $Rh_2(form)_4[C(CN)_3]$ with the corresponding atom-labeling scheme is shown in Figure 1. In Figure 2, the molecular spacefill is reported along the intermetallic axis, i.e., the 4-fold axis of symmetry parallel to the crystallographic *c*-axis, showing both of the two possible TCM dispositions (50% occupancy, considering that the atoms N(3), C(16), and C(17) are on the axis).

Results and Discussion

When complex **I** reacts with the above-named polycyano ligands, no redox reactions occur. On the contrary, the reactions proceed *via* axial coordination with a negligible degree of charge transfer from the dimetal unit to the ligand. Furthermore, according to the polyfunctional nature of **I** and the ligands TCNQ, 2,5-DMDCNQI, and NCNQI, the reactions of **I** with these ligands lead to polymeric materials while the reaction with TCNE results in the formation of a labile monoaxial adduct. In fact, by reacting the dirhodium(II) formamidinate species $Rh_2(form)_2(O_2CCF_3)_2(H_2O)_2$ with TCNE, a complex which analyzes as $Rh_2(form)_2(O_2CCF_3)_2$TCNE was obtained. The reaction is rapid and was followed by the formation of a precipitate when benzene is used as a solvent. The use of a different molar ratio does not alter the nature or the yields of the product. Complex **1** is diamagnetic and not conducting in acetonitrile. In a few minutes it dissolves in almost all of the solvents, leading to deeply colored solutions whose color is dependent on the solvent used. They are pink-red in acetonitrile, green in diethyl ether, brown in acetone, and yellow in dimethyl sulphoxide. This may be explained in terms of an equilibration between the TCNE weakly bonded to the dirhodium unit and

Table 3. Selected Interatomic Distances (Å) and Angles (deg) for $Rh_2(form)_4[C(CN)_3]$

Bond Distances

Rh(1)−Rh(2)	2.463(4)	Rh(2)−N(3)	2.07(3)
Rh(1)−N(1)	2.03(1)	Rh(2)−N(2)	2.03(1)
C(1)−N(1)	1.42(1)	C(7)−N(2)	1.45(1)
C(15)−N(1)	1.32(2)	C(15)−N(2)	1.33(1)
C(4)−C(13)	1.50(2)	C(10)−C(14)	1.49(2)
N(3)−C(16)	1.10(2)	C(16)−C(17)	1.55(4)
C(17)−C(18)	1.47(5)	C(18)−N(4)	1.12(3)

Angles[a]

N(2)−C(15)−N(1)	121(1)		
$N(1)^{i}$−Rh(1)−N(1)	89.9(1)	$N(1)^{ii}$−Rh(1)−N(1)	175.0(7)
$N(2)^{i}$−Rh(2)−N(2)	89.7(1)	$N(2)^{ii}$−Rh(2)−N(2)	172.0(7)
N(1)−Rh(1)−Rh(2)	87.5(3)	N(2)−Rh(2)−Rh(1)	86.0(3)
N(2)−Rh(2)−N(3)	94.0(3)	N(3)−Rh(2)−Rh(1)	180.0
C(15)−N(1)−C(1)	118(1)	C(15)−N(2)−C(7)	115(1)
C(15)−N(1)−Rh(1)	119(1)	C(15)−N(2)−Rh(2)	121(1)
C(1)−N(1)−Rh(1)	123(1)	C(7)−N(2)−Rh(2)	124.5(8)
Rh(2)−N(3)−C(16)	180.0	N(3)−C(16)−C(17)	180.0
C(18)−C(17)−C(16)	120(3)	N(4)−C(18)−C(17)	133(7)
$C(18)^{i}$−C(17)−C(18)	75(3)	$C(18)^{ii}$−C(17)−C(18)	120(6)
C(2)−C(1)−N(1)−C(15)	141(1)	C(8)−C(7)−N(2)−C(15)	116(2)
C(1)−N(1)−C(15)−N(2)	164(1)	N(1)−C(15)−N(2)−C(7)	172(1)

[a] Symmetry operators: (i) $y,-x+{}^1/_2, z$; (ii) $-x+{}^1/_2, -y+{}^1/_2, z$.

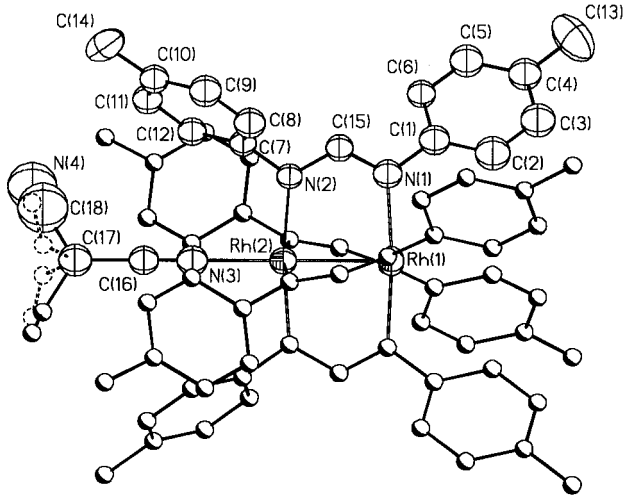

Figure 1. View of the complex $Rh_2(form)_4[C(CN)_3]$ showing both of the two possible orthogonal dispositions of $[C(CN)_3]^-$ and the numbering scheme of the asymmetric unit. Thermal ellipsoids are drawn at 25% probability, while hydrogen atoms are omitted for clarity.

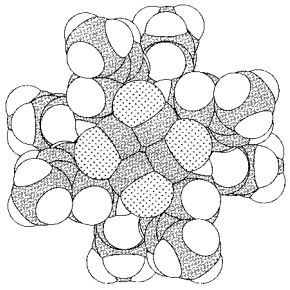

Figure 2. Space filling representation of the complex $Rh_2(form)_4[C(CN)_3]$ projected along *c* and showing both of the dispositions of the $[C(CN)_3]^-$ anion.

(12) Sheldrick, G. M. *SHELXL93. Program for Crystal Structure Refinement*; University of Göttingen: Germany, 1993.
(13) *International Tables for X-ray Crystallography*; Kynoch Press: Birmingham, 1974, Vol. IV.
(14) Nardelli, M. *Comput. Chem.* **1983**, *7*, 95 (version locally modified).

the solvent (or the water present in the solvent). It is well-known that TCNE, appropriately named the *Escherichia coli* of the chemistry,[15] interacts with transition metal complexes giving a variety of bonding arrangements unknown for other molecules. In its neutral form, it may be π-bonded, monodentate, 1,1- or 1,2-exobidentate and $\mu^4-\epsilon^4$ bridged *via* σ-coordination of one or all of its nitrile groups.[16] When it adopts the monodentate coordination, due to the poor σ-nucleophilicity of neutral TCNE, the resulting complexes are labile. On dissolution in coordinating or noncoordinating solvents, complex **1** easily dissociates, restoring the precursor which exhibits the well-known axial reactivity. Accordingly, the UV−vis spectrum is the sum of the absorption spectra of the constituent compounds. The solid IR spectrum of **1** shows strong ν(CN) absorptions at 2237 and 2202 cm^{-1}, namely very close to the values exhibited by the free ligand. Since the stretching frequency of the CN groups in these cyano ligands is representative of the degree of charge transfer,[17] it may be deduced that the reaction leading to **1** does not involve an appreciable charge transfer on TCNE and that the cyano ligand is coordinated to the dirhodium(II) core in a neutral form.

On the basis of the analytical data, complex **1** could correspond to either one-dimensional linear chains of $Rh_2(form)_2(O_2CCF_3)_2$ fragments linked by the TCNE ligand, acting as an exobidentate ligand, or to a simple monoaxial adduct. Although a polymer of formula $[Rh_2(O_2CCH_3)_4$-TCNE$]_n$[18] has been recently reported by Cotton, the high solubility of **1**, as well as the lability of the cyano ligand, leads us to suggest that **1** adopts a monomeric rather than a polymeric structure.

As previously cited, TCNQ, 2,5-DMDCNQI, and NCNQI react with **I** giving polymeric materials. The only difference lies in the stoichiometry and, hence, in the structure of the complexes. In fact, when **I** is allowed to react with the ligands TCNQ, 2,5-DMDCNQI, and NCNQI, low-soluble materials, corresponding to the empirical formula $\{[Rh_2(form)_2(O_2CCF_3)_2]_2$-TCNQ$\}_n$ (**2**) and $[Rh_2(form)_2(O_2CCF_3)_2X]_n$ (X = 2,5-DMDCNQI (**3**), NCNQI (**4**), respectively, were obtained. Solid-state IR spectra of **2** show, in addition to the bands associated with the formamidinate and trifluoroacetate fragments, ν(CN) absorption at 2215 cm^{-1}, slightly shifted to lower wavenumbers when compared to those of the free neutral TCNQ molecule and comparable to those observed for other neutral TCNQ complexes,[19] indicating that, again, the metal-to-ligand charge transfer process is negligible. A medium band at 863 cm^{-1}, observed in the spectrum of **2**, is a further confirmation of the neutral nature of TCNQ.[20] The ν(CN) of complexes **3** and **4** is very weak and cannot be confidently assigned.

Concerning the structures of **2**, **3**, and **4**, we suggest, on the basis of the analytical data, that **2** corresponds to a two-dimensional polymer in which TCNQ employs all four of its CN groups, acting as a $\mu^4-\epsilon^4$ bridging ligand, similar to the compound reported by Cotton[21] by reacting $Rh_2(O_2CCF_3)_4$ and TCNE, while compounds **3** and **4** may be best described as linear-chain polymers.

The reaction of $Rh_2(form)_4$ with 1 equiv of TCNE, TCNQ, or 2,5-DMDCNQI proceeds *via* a single electron transfer. It results in the formation of charge transfer species of the general formula $[Rh_2(form)_4X]$ (X = TCNE (**5**), TCNQ (**6**), 2,5-DMDCNQI (**7**)) containing the $[Rh_2(form)_4]^{\bullet+}$ cation radical and the cyano ligand as a radical anion. They are stable as solids, showing a moderate stability in solution. The structure of complexes **5**−**7** was inferred from a combination of UV−vis−near-IR and IR spectroscopic data and electrochemical measurements. Furthermore, being paramagnetic, they were also identified by EPR spectroscopy. These techniques have been extensively used in the characterization of CT-TCNX (X = E, Q) salts, as they provide significant information on the oxidation state, symmetry, and intermolecular interactions among TCNX radical anions. Solid-state infrared spectra of **5** and **6** show, in the 2000−2300 cm^{-1} region, absorptions at 2198 and 2154 and 2193 and 2163 cm^{-1}, respectively. A comparison of the nitrile stretching frequencies of **5** and **6** with those reported in the literature for $TCNE^{\bullet-}$ [22] and $TCNQ^{\bullet-}$ [23] containing complexes can be used to confirm that the cyano ligands are present as negative radical species. This means that the reactions leading to **5** and **6** proceed by a complete electron transfer from the donor complex $Rh_2(form)_4$ to the acceptor molecules. The observation of a medium-intensity band at 825 cm^{-1}, assigned to the out-of-plane C−H bending, is a further indication of the presence of the $TCNQ^{\bullet-}$ species in complex **5**.[20] Comparison between the solid IR spectra of **1** and **2** with those of **5** and **6** evidences the low-frequency shift of the ν(CN) of **5** and **6** with respect to those of **1** and **2**, in agreement with the increased degree of electron transfer from complex **II** to the π-accepting ligand.

The features observed in the UV−vis−near-IR spectra may be considered definitive evidence of the presence of TCNE and TCNQ in their reduced forms. The electronic spectra of complex **5** in CH_3CN or THF show structured absorptions with a maximum at 428 nm and a broad intense near-IR band at 910 nm. The higher energy absorption, characterized by a fine structure due to several vibrational overtones, is diagnostic of the $TCNE^{\bullet-}$ radical anion,[24] while the absorption at 910 nm, which is also present in the complex $[Rh_2(form)_4]O_2CCF_3$, is confidently assigned as a ligand-to-metal charge transfer (LMCT) process by analogy to similar derivatives.[25] Complex **6** shows two absorptions, one with a maximum at 842 nm and the other one, less intense, with a maximum at 420 nm. Frequency and shape of these bands are as found in simple salts or complexes containing the species $TCNQ^{\bullet-}$.[26]

Conductivity measurements show that in acetonitrile **5** and **6** behave as 1:1 electrolytes, while in tetrahydrofuran, they are not conducting. These data may be interpreted in terms of a dissociation of the cyano ligand that is dependent on the polarity of the solvent, so that the species operating in acetonitrile are the CT salts $[Rh_2(form)_4]^{\bullet+}X$ (X = $TCNE^{\bullet-}$, $TCNQ^{\bullet-}$), while in nondissociating solvents, the cyano ligands are coordinated as radical anions to the Rh_2^{5+} core through the nitrogen atom of a cyano group. Previous X-ray studies[1b] evidenced that

(15) Olbrich-Deussner, B.; Kaim, W.; Gross-Lannert, R. *Inorg. Chem.* **1989**, *28*, 3113 and references therein.
(16) Kaim, W.; Moscherosh, M. *Coord. Chem. Rev.* **1994**, *129*, 157.
(17) (a) Chappel, J. S.; Bloch, A. N.; Bryden, W. A.; Maxfield, M.; Poehler, T. O.; Cowan, D. O. *J. Am. Chem. Soc.* **1981**, *103*, 2442. (b) Beck, W.; Schlodder, R.; Lecher, K. H. *J. Organomet. Chem.* **1973**, *5*, 303.
(18) Cotton, F. A.; Kim, J.; Lu, J. *Inorg. Chim. Acta* **1994**, *221*, 1.
(19) Pace, L. S.; Ulman, A.; Ibers, J. A. *Inorg. Chem.* **1982**, *21*, 199.
(20) (a) Lunelli, R.; Pecile, C. *J. Chem. Phys.* **1970**, *52*, 2375. (b) Pukaki, W.; Pawlak, M.; Graja, A.; Lequan, M.; Lequan, R. M. *Inorg. Chem.* **1987**, *26*, 1328.
(21) Cotton, F. A.; Kim, Y. *J. Am. Chem. Soc.* **1993**, *115*, 8511.
(22) Olbrich-Deussner, B.; Gross, R.; Kaim, W. *J. Organomet. Chem.* **1989**, *366*, 155.
(23) Bell, S. E.; Field, J. S.; Haines, R. J.; Moscherosch, M.; Matheis, W.; Kaim, W. *Inorg. Chem.* **1992**, *31*, 3269.
(24) (a) Dixon, D. A.; Miller, J. S. *J. Am. Chem. Soc.* **1987**, *109*, 3656. (b) Webster, O. W.; Mahler, W.; Benson, R. E. *Ibid.* **1962**, *84*, 3678.
(25) Bear, J. L.; Yao, C. L.; Liu, M. L.; Capdevielle, F. J.; Korp, J. D.; Albright, T. A.; Kang, S. K.; Kadish, K. M. *Inorg. Chem.* **1989**, *28*, 1254.
(26) Melby, R. L.; Harder, R. J.; Hertler, W. R.; Mahler, W.; Benson, R. E.; Mochel, W. E. *J. Am. Chem. Soc.* **1962**, *84*, 3374.

despite the overcrowding of the axial positions of the complex $Rh_2(form)_4$, due to the presence of four *p*-tolyl groups, small or linear molecules can coordinate at the axial positions. Furthermore, the one-electron oxidation causes a more favorable disposition of the *p*-tolyl groups around one axial position.[4b] It is not surprising that TCNX ligands, before or after the redox process, are able to enter into the coordination sphere of the metal. Further support of this suggestion comes from the EPR spectroscopy (see later).

Redox reactions between transition metal complexes and TCNX (X = E, Q) ligands, leading to charge transfer salts with the $TCNX^{\bullet-}$ anion in the outher coordination sphere of the metal, are not uncommon, and the metallocene derivatives are the most representative for this class of reactions.[24a,27] The complex $Rh_2(form)_4$, owing to the presence of open coordination sites and appropriate redox potentials, is one of the few examples of metal complexes able to accomplish both reduction and coordination (or coordination and reduction) of TCNX cyano ligands.[23,28]

Although the reaction between $Rh_2(form)_4$ and 2,5-DMDCNQI belongs to the class of reactions just described, we like to discuss it separately because the reactivity of *N*,*N*′-dicyano-*p*-quinonediimmines, both in their neutral or monoreduced form, with metal complexes is virtually unknown. The only report deals with the complex $(\eta^5\text{-}C_5Me_5)Mn(CO)_2(\eta^1\text{-}2,5\text{-}DMDCNQI)$, in which, due to its lability, only solid-state infrared and UV spectral data are reported.[15] In contrast to the wealth of experimental and theoretical studies available for TCNX systems, literature data are not of much help in assigning the structure and formal oxidation number of DCNQI derivatives. The complex $Rh_2(form)_4$ easily reacts with 1 equiv of 2,5-DMDCNQI, giving a blue solution from which a complex which analyzes as $Rh_2(form)_4$(2,5-DMDCNQI) was recovered in a good yield. Contrary to from **5** and **6**, complex **7** is stable both in solution and as a solid. Conductivity measurements carried out in acetone show that it behaves as a nonelectrolyte, while in CH_3CN, it is partially dissociated. This suggests that in complex **7**, the cyano ligand is σ-coordinated at one axial position of the species $[Rh_2(form)_4]^{\bullet+}$ and that this interaction is stronger than that in the TCNE and TCNQ derivatives. The solid-state IR spectrum of **7** exhibits a single ν(CN) at 2134 cm^{-1}, while the visible spectrum consists of two high-intensity bands at 696 and 628 nm and a broad band at 933 nm. The first two bands are shifted to higher energy in CH_3CN, where **7** is partially dissociated. Except for the latter band, the IR and UV−vis spectral data are comparable with those of the previously cited complex $(\eta^5\text{-}C_5Me_5)Mn(CO)_2(\eta^1\text{-}2,5\text{-}DMDCNQI)$. However, they do not allow us to assess that the reaction leading to **7** occurs through an electron transfer step and that in complex **7** is present the species $[2,5\text{-}DMDCNQI]^{\bullet-}$. Only the absorption at 933 nm, assigned as a LMCT, suggests the presence of the $[Rh_2(form)_4]^{\bullet+}$ cation radical. More convincing information on the structure of **7** was obtained by EPR spectroscopy.

Attempts to crystallize compound **5** from acetonitrile resulted, after 7 days, in the formation of a new compound, which analyzes as $Rh_2(form)_4[C(CN)_3]$ (**5A**). This species exhibits, in the IR spectrum, ν(CN) bands at 2180 and 2220 cm^{-1}. We attempted to characterize this compound by relating it to literature of cyano carbons and found that these values compare reasonably well with the peak in the $KC(CN)_3$ spectrum at 2178 cm^{-1}.[29] To support the formulation of **5A** as a tricyanomethanide derivative, the complex $[Rh_2(form)_4]ClO_4$ was allowed to react with $K[C(CN)_3]$ in a 1:1 molar ratio. The reaction product exhibits the same analytical and spectroscopic data as **5A**, confirming the nature of the cyano ligand. The unequivocal identity of the title complex was ascertained by the X-ray analysis, which shows the presence of a coordinated tricyanomethanide group. It is well-recognized that TCNE in its reduced form may undergo transformations giving a variety of cyano ligands as reactive species. In particular, the tetracyanoethylenide ion has been observed to react with oxygen or water to give pentacyanopropenide[27c,28b,30] or tricyanoethanolate ions, respectively.[31] It can also transform into the $[C_4(CN)_6]^{2-}$ anion, as well as disproportionate into $TCNE^{2-}$ and TCNE.[32] Its transformation into the tricyanomethanide ion has not been previously reported.

The process by which the $[C(CN)_3]^-$ species is formed is clearly unknown, and we do not feel confident to make unsupported speculations. Moreover, as the synthesis and workup of complex **5A** was accomplished both in air as well as under a purified nitrogen atmosphere, we can exclude the possibility that the formation of the $[C(CN)_3]^-$ anion is caused by air.

X-ray Structure of $Rh_2(form)_4[C(CN)_3]$. The crystal structure of the title compound, as shown in Figure 1, consists of discrete $Rh_2(form)_4[C(CN)_3]$ molecules packed together by van der Waals interactions. The molecule consists of a dirhodium unit symmetrically bridged by four formamidinate (form) ligands and one tricyanomethanide anion (TCM) N-coordinated at the axial position of Rh(2). The molecule lies on the crystallographic 4-fold axis of symmetry passing through the metal centers and the TCM ligand. Therefore, the crystallographic asymmetric unit is represented by a Rh−Rh−form unit, while the TCM anion is perfectly distributed on two possible orthogonal dispositions generated by the 4-fold axis of symmetry (Figure 2). The tetragonal crystal packing of the solid is mainly determined by the symmetry of the $Rh_2(form)_4$ moiety.

Due to the steric hindrance of the four *p*-tolyl fragments surrounding the axial coordination site, the TCM anion adopts the N-coordination instead of the C-interaction, *via* the hybridized sp^3 carbon. The N-coordination, observed in compounds where the ionic interaction is important,[33] is associated with the perfect sp^2 hybridization of the central carbon atom that allows the planar arrangement of the TCM anion, in agreement with the symmetry requirements. Indeed, in other N-coordinated tricyanomethanide derivatives,[34] a slight pyramidalization of the central carbon has been found.

(27) (a) Ward, M. D.; Johnson, D. C. *Inorg. Chem*. **1987**, *26*, 4213. (b) Murphy, V. J.; O'Hare, D. *Inorg. Chem*. **1994**, *33*, 1833. (c) Eichhorn, D. M.; Skee, D. C.; Broderick, W. E.; Offmann, B. M. *Inorg. Chem*. **1993**, *32*, 491. (d) Miller, J. S.; Calabrese, J. C.; Harlow, R. L.; Dixon, D. A.; Zhang, J. H.; Reiff, W. M.; Chittipeddi, S.; Selover, M. A.; Epstein, A. J. *J. Am. Chem. Soc.* **1990**, *112*, 5496. (c) Miller, J. S.; Calabrese, J. C.; Rommelmann, H.; Chittipeddi, S. R.; Zhang, J. H.; Reiff, W. M.; Epstein, A. J. *J. Am. Chem. Soc*. **1987**, *109*, 769.

(28) (a) Gross-Lannert, R.; Kaim, W.; Olbrich-Deussner, B. *Inorg. Chem*. **1990**, *29*, 5046. (b) Giraudon, J. M.; Sala-Pala, J.; Guerchais, J. E.; Toupet, L. *Inorg. Chem*. **1991**, *30*, 891. (c) Bartley, S. L.; Dunbar, K. R. *Angew. Chem., Int. Ed. Engl*. **1991**, *30*, 48.

(29) Miller, F. A.; Baer, W. K. *Spectrochim. Acta* **1963**, *19*, 73.

(30) (a) Bruce, M. I.; Wallis, R. C.; Skelton, W. B.; White, A. H. *J. Chem. Soc., Dalton Trans*. **1981**, 2205.

(31) Sullivan, B. W.; Foxman, B. M. *Organometallics* **1983**, *2*, 187.

(32) (a) Beck, W.; Schlodder, R.; Lecher, K. H. *J. Organomet. Chem*. **1973**, *5*, 303. (b) Yee, G. T.; Calabrese, J. C.; Vasquez, C.; Miller, J. S. *Inorg. Chem*. **1993**, *32*, 377.

(33) (a) Beck, W.; Hieber, W.; Neumair, G. *Z. Anorg. Allg. Chem.* **1966**, *344*, 185. (b) Köhler, H.; Hartung, H.; Seifert, B. *Z. Anorg. Allg. Chem.* **1966**, *347*, 30. (c) Lenarda, M.; Baddley, W. H. *J. Organomet. Chem*. **1972**, *39*, 217.

(34) Wang, J.-C; Shih, L. J.; Chen,Y.-J.; Wang, Y.; Fronczek, F. R.; Watkins, S. F. *Acta Crystallogr*. **1993**, *B49*, 680.

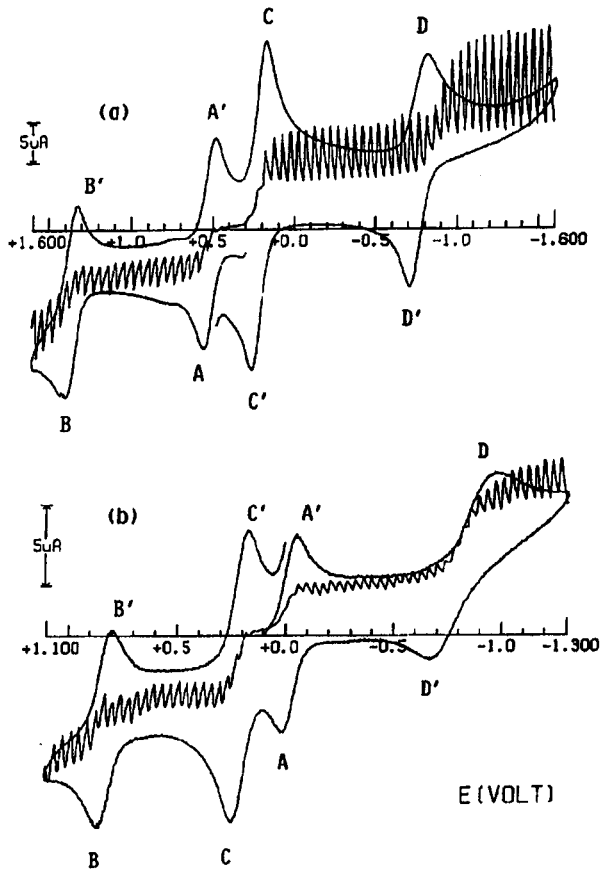

Figure 3. CV and DCV responses recorded at a platinum electrode on MeCN solutions containing $[NEt_4][ClO_4]$ (0.1 mol dm^{-3}) and: (a) **1** (0.8×10^{-3} mol dm^{-3}); (b) **5** (0.4×10^{-3} mol dm^{-3}). Scan rates: CV, 0.2 Vs^{-1}; DCV, 0.02 Vs^{-1}.

The presence of a TCM coordinated at the axial position of Rh(2) is responsible of the different geometry adopted by the two rhodium atoms, which is pseudo-octahedral for Rh(2) and a square pyramidal for Rh(1) having the axial site empty. The different coordination number also causes the elongation of the Rh(2)−N(2) bond with respect to the Rh(1)−N(1) bond, while the bond angles between opposite nitrogens are 175.0(7)° and 172.0(7)° for N(1)−Rh(1)−N(1)′ and N(2)−Rh(2)−N(2)′, respectively.

The Rh−Rh bond length (2.463(4) Å) as well as the structural parameters associated with the formamidinate anions are comparable with the corresponding values found in the complex $[Rh_2(form)_4(H_2O)]O_2CCF_3$.[4b] The steric hindrance of the axial ligand causes a distorsion of the formamidinate arrangement, which is apparent from the deviation from the plane through N(1)C(15)N(2) and from the N−Rh−Rh−N torsion angle (16.9(6)°), which is smaller than that of the previous complex (18.1(3)°). As a consequence, the four formamidinate ligands assume a screw-like arrangement around the intermetallic axis, i.e., the crystallographic 4-fold axis, with the *p*-tolyl fragments attached to N(2) being more rotated to allow the coordination of TCM to Rh(2) along the same axis. In agreement with the trend observed in the complex $[Rh_2(dpf)_4(CH_3CN)]ClO_4$ (dpf = diphenylformamidinate),[35] the axial nitrogen ligand differentiates the N−C(*p*-tolyl) bonds (1.42(1) and 1.45(1) Å, respectively) while the Rh(2)−N(axial) bond lengths of 2.07(3) Å are comparable. The Rh(1)−Rh(2)−N(3) bond angle is determined (180°) by the symmetry requirement.

(35) Bear, J. L.; Yao, C.-L.; Lifsey, R. S.; Korp, J. D.; Kadish, K. M. *Inorg. Chem.* **1991**, *30*, 336.

Table 4. Formal Electrode Potentials (V, vs SCE) for the Redox Changes Exhibited by the Precursors of the Charge-Transfer Complexes Presented here in Different Solvents

complex	$E^{\circ\prime}_{+/2+}$	$E^{\circ\prime}_{0/+}$	$E^{\circ\prime}_{0/-}$	$E^{\circ\prime}_{-/2-}$	solvent
$Rh_2(form)_4$	+0.81	0.00	<−1.9		MeCN[a,b]
	+0.95	+0.12	−1.43		CH_2Cl_2[c]
	d	+0.31	−1.27		THF[c]
$Rh_2(form)_2(O_2CCF_3)_2$	+1.37	+0.53			MeCN[b]
	+1.40	+0.59			CH_2Cl_2[c]
TCNE			+0.23	−0.74	MeCN[b]
			+0.25	-0.79	CH_2Cl_2[c]
			+0.25	−0.83	THF[c]
TCNQ			+0.19	−0.34	MeCN[b]
			+0.18	−0.40	CH_2Cl_2[c]
			+0.29	−0.40	THF[c]
2,5-DMDCNQI			+0.06	−0.57	MeCN[b]
			−0.02	−0.62	CH_2Cl_2[c]
			+0.14	−0.61	THF[c]
$[C(CN)_3]^-$			+1.28[e]		MeCN[b]
			+1.33[e]		THF[c]
			+1.22[e]		CH_2Cl_2[c]

[a] Very slightly soluble. [b] $[NEt_4][ClO_4]$ (0.1 mol dm^{-3}) supporting electrolyte. [c] $[NBu_4][PF_6]$ (0.2 mol dm^{-3}) supporting electrolyte. [d] Ill-defined process. [e] Peak-potential value measured at 0.2 Vs^{-1}.

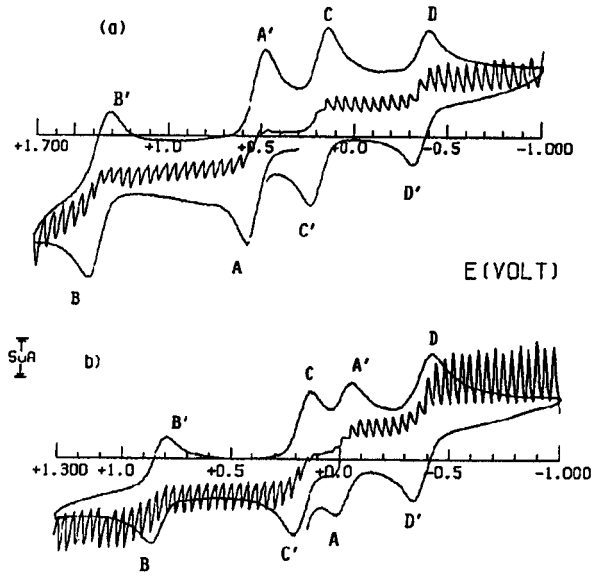

Figure 4. CV and DCV responses recorded at a platinum electrode on MeCN solutions containing $[NEt_4][ClO_4]$ (0.1 mol dm^{-3}) and: (a) **2** (0.3×10^{-3} mol dm^{-3}); (b) **6** (0.4×10^{-3} mol dm^{-3}). Scan rates: CV, 0.2 Vs^{-1}; DCV, 0.02 Vs^{-1}.

Electrochemistry. Figure 3 compares the electrochemical responses of **1** and **5** in an acetonitrile solution, both in cyclic voltammetry (CV) and in direct current voltammetry (DCV) at an electrode with a periodical renewal of the diffusion layer.

As shown in Figure 3a, complex **1** undergoes two subsequent oxidations as well as two subsequent reductions that are chemically reversible. As deducible from Table 4, the oxidation processes A and B occur at potential values coincident with those of free $Rh_2(form)_2(O_2CCF_3)_2$ as, on the other hand, the reduction processes C and D do with respect to free TCNE. As expected on the basis of their diffusion coefficients, the limiting current for the redox changes of TCNE is significantly higher than that of the dirhodium fragment ($i_{lim(Rh_2)}/i_{lim(TCNE)} \cong 0.6$). These data agree with the formulation of **1** as $[Rh_2(form)_2(O_2CCF_3)_2TCNE]$. As shown in Figure 4a, complex **2** exhibits, in acetonitrile solution, a redox profile similar to that of **1**, thus, confirming that no redox process takes place on mixing the two components. In addition, in agreement with the 2:1 (Rh_2:TCQM) stoichiometry, the limiting currents of the oxidation

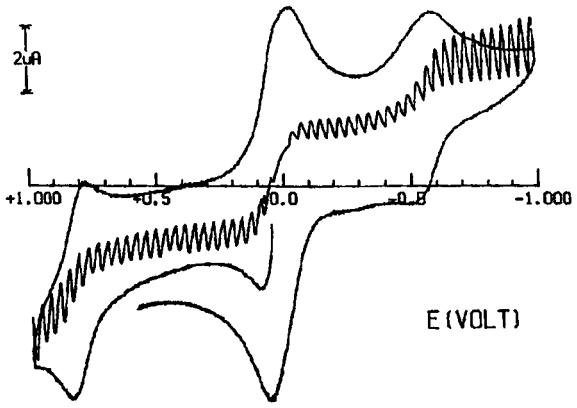

Figure 5. CV and DCV responses recorded at a platinum electrode on a MeCN solution containing **7** (0.2×10^{-3} mol dm^{-3}) and [NEt_4][ClO_4] (0.1 mol dm^{-3}). Scan rates: CV, 0.2 Vs^{-1}; DCV, 0.02 Vs^{-1}.

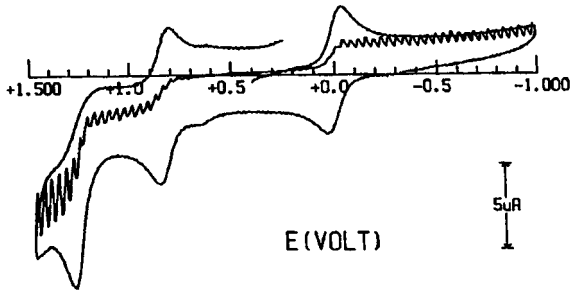

Figure 6. CV and DCV responses recorded at a platinum electrode on a MeCN solution containing **5A** (0.3×10^{-3} mol dm^{-3}) and [NEt_4][ClO_4] (0.1 mol dm^{-3}). Scan rates: CV, 0.2 Vs^{-1}; DCV, 0.02 Vs^{-1}.

processes of the dirhodium component are slightly higher than those of the reductions of TCQM ($i_{lim(Rh_2)}/i_{lim(TCQM)} \cong 1.2$).

By contrast, on the basis of either the formal electrode potentials or the relative limiting currents ($i_{1im(Rh_2)}/i_{lim(TCNE)} \cong 0.8$), it is deducible from Figure 3b that the first anodic step C of complex **5** has to be assigned to the $TCNE^-$/TCNE oxidation, whereas the first cathodic step A′ has to be assigned to the $[Rh_2(form)_4]^+/Rh_2(form)_4$ reduction. The processes B/B′ and D/D′ maintain the previous assignment. In turn, as illustrated in Figure 4b, the redox responses of **6**, in acetonitrile solution ($i_{lim(Rh_2)}/i_{lim(TCQM)} \cong 0.8$), parallel those of **5**, with the anodic step C′ assigned to the $TCQM^-$/TCQM oxidation. These data confirm that the reactions leading to **5** and **6** occur through a complete electron transfer from the donor parent complex to the cyano ligands.

In acetonitrile solution, complexes **3** and **4** behave like **1**.

The electrochemical behavior of complex **7** is less easily interpretable since, as shown in Figure 5, the first oxidation overlaps the first reduction, thus, giving rise to a catho-anodic DCV response; this is in agreement with the close potential values of the two redox couples $[Rh_2(form)_4]^+/Rh_2(form)_4$ and 2,5-DMDCNQI/[2,5-DMDCNQI]$^-$.

Finally, Figure 6 shows the voltammetric profile of **5A** in acetonitrile solution. The complex displays the $[Rh_2(form)_4]^+/Rh_2(form)_4$ reduction together with the $[Rh_2(form)_4]^+/[Rh_2(form)_4]^{2+}$ oxidation. The irreversible process at $E_p = +1.28$ V is due to the oxidation of the $[C(CN)_3]^-$ monoanion. In this picture, according to the conductivity measurements, in acetonitrile solution the formulation of **5A** as [$Rh_2(form)_4$][$C(CN)_3$] is confirmed. By contrast, Figure 7 shows the voltammetric profile of **5A** in tetrahydrofuran solution.

The first dirhodium reduction (peak system A/D) occurs at −0.04 V, i.e., at a potential value more cathodic by about 0.35 V with respect to that of the uncoordinated complex. The fact

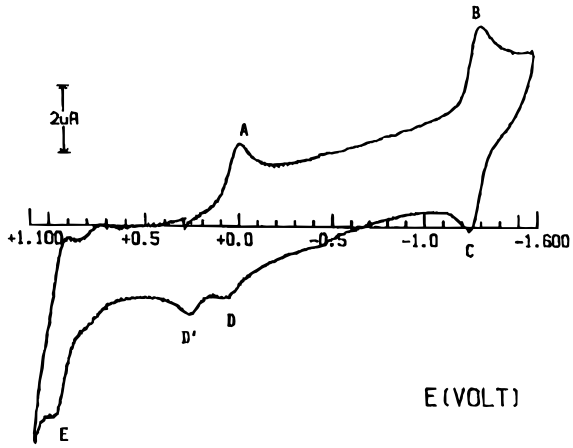

Figure 7. Cyclic voltammetric response recorded at a platinum electrode on a THF solution containing **5A** (0.3×10^{-3} mol dm^{-3}) and [NBu_4][PF_6] (0.2 mol dm^{-3}). Scan rate, 0.2 V s^{-1}.

that the second reduction step (peak system B/C) is localized at a potential value coincident with that of the second reduction of free $Rh_2(form)_4$, as well as the oxidation peak of free $Rh_2(form)_4$ (peak D′, $E_p \cong +0.3$ V), suggests that, at least in the cyclic voltammetric scale, the one-electron reduction causes decoordination of the $C(CN)_3$ group. The i_{pD}/i_{pA} ratio significantly lower than unity confirms the presence of chemical complications coupled to the first reduction. In conclusion, the electrochemical response suggests the presence of a strong coordination of the $[C(CN)_3]^-$ monoanion to the $[Rh_2(form)_4]^+$ fragment, thus, likely accounting for the nonconductivity of **5A** in tetrahydrofuran solution.

Attempts to record the cyclic voltammetric responses of all of the other complexes in noncoordinating dichloromethane or tetrahydrofuran solutions afforded irreproducible results. Only complex **1** was stable in dichloromethane solution. It displays a redox pattern qualitatively similar to that shown in Figure 3a, except for the fact that the first Rh_2 oxidation occurs at potential values that are higher by 50 mV and the first TCNE reduction occurs at potential values that are lower by 30 mV, with respect to the corresponding processes for free precursors. This suggests that a weak coordination of neutral TCNE to the neutral dirhodium fragment is likely present in the complex.

As a final comment to the electrochemical investigation, it is worth mentioning that the data compiled in Table 4 indicate that depending on the solvent, the redox properties of TCNE, TCNQ, and 2,5-DMDCNQI should be insufficient to ensure the oxidation of **II**. It is evident that under synthetic nonstandard conditions, the barrier to electron transfer is overcome.

EPR Measurements. Complexes **5**−**7** display similar X-band EPR features. As a typical example, Figure 8a shows the X-band EPR spectrum of the microcrystalline powder of **5** at liquid nitrogen temperature. Two distinct absorption patterns are evident in the line shape analysis with very different spectral intensities. The more intense one displays a well-resolved rhombic structure, while the second one is slightly axial. Both of the signals can be suitably interpreted assuming the presence of two noninteracting and separately relaxing paramagnetic systems, each one characterized by a proper anisotropic $S = {}^1/_2$ electron spin Hamiltonian. The corresponding line shapes have been suitably computed,[36] and the relevant best fit parameters are summarized in Table 5. The broad rhombic signal can be assigned to the paramagnetic $S = {}^1/_2$ $[Rh_2(form)_4]^{\bullet+}$ fragment with $g_i \neq g_e = 2.0023$, which well reflects the metal-in character of the overall spectrum. The actual EPR features are consistent

(36) Lozos, J. P.; Hoffman, B. M.; Franz, C. G. *QCPE* **1973**, *11*, 243.

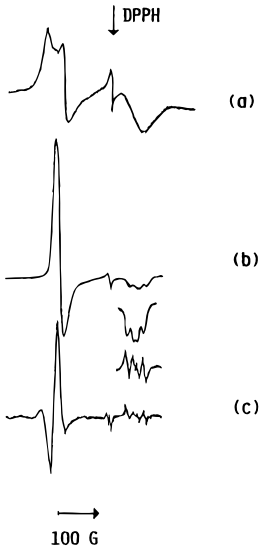

Figure 8. X-band EPR spectra of **5** under the following experimental conditions: (a) microcrystalline powder at $T = 100$ K; (b,c) CH_2Cl_2 solution at $T = 100$ K, first-derivative mode and second-derivative mode, respectively.

Table 5. X-Band EPR Parameters of Complexes **5**−**7** under Different Experimental Conditions

complex	fragment	fnt	g_l[a]	g_m[a]	g_h[a]	$\langle g\rangle$[a,b]	a_h[c]	g_{iso}[d]	a_{iso}[e]
5	Rh_2	*f*	2.106	2.074	1.966	2.049	≤30		
		g	2.103	2.075	1.957	2.044	≤30		
		h	2.078	2.078	1.963	2.040	26 15	2.043	≤28
		i	2.081	2.081	1.961	2.041	22	2.047	≤28
		l	2.079	2.079	1.964	2.041	18	2.045	≤30
	TCNE	*f*	2.004	2.001	2.001	2.002			
		g	2.005	2.001	2.001	2.002			
		h	2.006	2.001	2.001	2.002		2.0022	1.6
		i	2.008	2.004	2.004	2.005		2.0024	1.6
		l	1.998	1.998	1.998	1.998		2.0018	1.6
6	Rh_2	*f*	2.104	2.059	1.946	2.036	≤40		
		g	2.101	2.060	1.948	2.036	≤40		
		h	2.081	2.081	1.960	2.040	22	2.046	≤28
		i	2.065	2.065	1.955	2.028	25	2.034	≤28
	TCQM	*f*	2.006	2.002	2.002	2.003			
		g	2.004	1.999	1.999	2.001			
		i	1.996	1.996	1.996	1.996		1.9990	1.2
		l	2.004	2.004	2.004	2.004		2.0036	*m*
7	Rh_2	*f*	2.070	2.070	1.955	2.032	*n*		
		g	2.060	2.060	1.964	2.028	*n*		
		i	2.081	2.081	1.952	2.038	*n*	2.050	≤30
		o	2.079	2.079	1.950	2.036	*n*	2.060	≤30
	DCNQI	*f*	2.011	2.006	2.006	2.008			
		g	2.005	2.005	2.005	2.005			
		i	2.007	2.007	2.007	2.007		2.0030	*i*
		o	2.004	2.004	2.004	2.004		2.0036	4.2
5A	Rh_2	*f*	2.091	2.070	1.960	2.043	≤30		
		h	2.072	2.072	1.964	2.036	20	2.043	≤30
		l	2.082	2.066	1.973	2.036	20	2.038	≤30

[a] ±0.004. [b] $\langle g\rangle = {}^1/_3(g_l + g_m + g_h) = {}^1/_3(g_{\|} + 2\,g_{\perp})$. [c] ±4 G. [d] Measured at 300 K; $g_{metal} = \pm 0.004$; $g_{radical} = \pm 0.0003$. [e] Measured at 300 K; $a_{metal} = \pm 4$ G; $a_{radical} = \pm 0.2$ G. [f] Microcrystalline powder, at 100 K. [g] Microcrystalline powder, at 300 K. [h] CH_2Cl_2 solution at 100 K. [i] THF solution at 100 K. [l] MeCN solution at 100 K. [m] Unresolved signal. [n] Not evaluable. [o] Acetone solution at 100 K.

with a mixed-valence Rh(II)−Rh(III) low-spin electronic structure in a distorted O_h geometry. The second-derivative spectrum displays a poor resolution of the high-field region, consistent with the presence of a broad doublet arising from the hyperfine coupling of the $S = {}^1/_2$ metal electron with one magnetically active rhodium nucleus (^{103}Rh; $I = {}^1/_2$; $a_h \leq 30$ G). The less intense, narrow intermediate signal diplays poorly separated and unresolved axial parameters, which verifies the presence of a $S = {}^1/_2$ organic radical ($\langle g\rangle_{TCNE^{\bullet-}} \cong g_e$), see Table 5. Because of minor H ($I = {}^1/_2$) and N ($I = 1$) anisotropic magnetic couplings ($a_{H,N(100K)} < \Delta H_{100K}$), no hyperfine (hpf) resolution is detectable.

When the temperature is increased, the two microcrystalline signals remain identical to the liquid nitrogen ones, confirming the stability of the molecular geometry of **5** in a wide range of temperatures. A slight line-broadening effect at 300 K may be explained in terms of a nonperfect stacking of the $TCNE^{\bullet-}$ radical anions, which, in the presence of a strong electron spin−electron spin interaction, should induce significant line narrowing.[37,38]

Figure 8b shows the liquid nitrogen X-band EPR spectra of **5** in dichloromethane solution. The $S = {}^1/_2$ spin Hamiltonian line shape analysis is consistent with the presence of two different paramagnetic systems, the former displaying significant metal-in axial features ($g_{\|} < g_e < g_{\perp}$) and the latter exhibiting a narrow and low-intensity line shape characteristic of the $TCNE^{\bullet-}$ radical in a slightly axial symmetry (see Table 5). Second-derivative line shape analysis of the metal pattern, Figure 8c, displays a well-resolved hpf doublet of doublets (1:1:1:1) in the $g_{\|}$ region. The $g_{\|}$ value of 1.963 ($< g_e$) is consistent with the main occupation of the δ^*_{Rh-Rh} orbital largely domining the SOMO, which is delocalized along the Rh_2 vector, even in the presence of different magnetic couplings with the two rhodium nuclei.[1b,4b,39] Such unsymmetrically distributed unpaired spin density[1b] proves that the $TCNE^{\bullet-}$ fragment is coordinated at one axial position of the dirhodium unit, thus, accounting for the actual anisotropic hpf couplings. The corresponding parameters, which are compiled in Table 5, are in good agreement with those in the solid state. Thus, this further confirms that the dirhodium unit maintains its geometry under different experimental conditions, even if the actual axial structure indicates that a more symmetric ligand field arrangement is experienced by the $S = {}^1/_2$ metal electron with respect to the corresponding microcrystalline rhombic pattern, a likely consequence of the absence of rigid crystal constraints.[40]

Under glassy solution conditions, the $TCNE^{\bullet-}$ radical displays spectral parameters identical with the microcrystalline ones.

When the temperature is increased, at the glassy−fluid transition phase, the two anisotropic signals drop out while two new isotropic absorptions appear, Figure 9a.

The corresponding EPR parameters are consistent with the presence of two different $S = {}^1/_2$ electron spin systems, the low-field one with metal-in character ($g_{iso(200K)} = 2.058$) and the high-field one being radical-type. Both of the spectra display a reversible increase of EPR intensities with temperature; in addition, the g_{iso} value of the dirhodium fragment exhibits high-field shifts. This spectral behavior indicates that in solution, the rising of temperature induces an effective averaging of the structural anisotropies of **5**. The concomitant shift of the g_{iso} value toward the g value of free $[Rh_2(form)_4]^{\bullet+}$ ($g_{iso} = 2.037$)[1b]

(37) Carrington, A.; McLachlan, A. D. *Introduction to Magnetic Resonance;* Harper and Row: New York, 1967.
(38) Cerrada, E.; Gimeno, M. C.; Laguna, A.; Laguna, M.; Orera, V.; Jones, P. G. *J. Organomet. Chem.* **1996**, *506*, 203.
(39) Kawamura, T.; Fukamachi, K.; Sowa, T.; Hayashida, S.; Yonezawa, T. *J. Am. Chem. Soc.* **1981**,*103*, 364.
(40) (a) Goodman, B. A.; Raynor, J. B. *Advances in Inorganic Chemistry and Radiochemistry*; Academic Press: New York, 1970; Vol. 13. (b) McGarvey, B. R. *NATO Advanced Study Institutes series*; D. Reidel Publisher Company: Dordrecht, 1980; Vol. 52. (c) Bianchini, C.; Peruzzini, M.; Laschi, F.; Zanello, P. *Topics in Physical Organometallic Chemistry*; Gielen, M. F. Ed.; Freund Publishing House LTD: London, 1992; Vol. 4, 139−219.

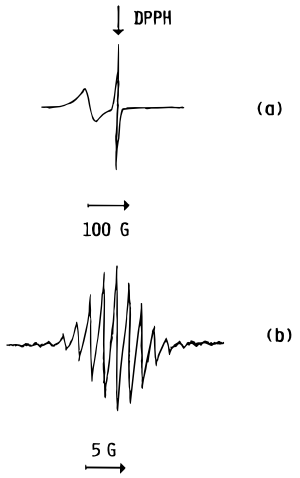

Figure 9. X-band EPR spectra of **5** in CH_2Cl_2 solvent at $T = 300$ K.(a) Absorption profile of the $[Rh_2(form)_4]^{\bullet+}$ fragment; (b) absorption profile of the $TCNE^{\bullet-}$ fragment.

suggests that the previously cited interaction between the $[Rh_2(form)_4]^{\bullet+}$ and $TCNE^{\bullet-}$ subunits decreases. No hpf features are evident, so that we can assume that: $a_{iso(300K)} \leq \Delta H_{iso(300K)} = 30$ G.

In fluid solution (178−300 K), the $TCNE^{\bullet-}$ signal exhibits a well-resolved hpf nonuplet (1:4:10:16:19:10:6:4:1) resulting from the isotropic magnetic coupling of the $S = {}^1/_2$ nonmetal electron with the four equivalent N nuclei, Figure 9b. Moreover, the fluid solution line shape displays, at the outer ends of the spectrum less intense but equally spaced hpf peaks indicative of the ^{13}C ($I = {}^1/_2$, 1.1% natural abundance) hpf satellite splittings resulting from the magnetically coupled $^{13}C-^{14}N$ system of the tetracyanoethylene radical, which largely overlaps with the most intense radical nonuplet. In spite of the fact that the actual $a_{iso(N)} = 1.6 \pm 0.2$ G is very similar to that of free $TCNE^{\bullet-}$ radical,[41] some line-broadening effects are present, likely due to a residual interaction with the dirhodium unit.

Upon changing the solvent, different spectral features appear in the glassy spectrum of **5**, which reflect the coordinating ability of the solvent toward the dirhodium fragment. In particular, while the noncoordinating dichloromethane behaves as a gas-phase-like solution, affording the best g_h region hpf resolution (doublet of doublets), acetonitrile solutions show a significant variation of the g_h region line shape. Here, broadened 1:2:1 pseudo-triplet or really triplet (MeCN; $a_h(Rh_2) = 18 \pm 4$ G) peaks are present, resulting from the hpf interaction of the $S = {}^1/_2$ metal electron with two nearly equivalent Rh nuclei. Such spectral features confirm that in acetonitrile **5** dissociates, affording the cation $[Rh_2(form)_4]^{\bullet+}$. In this species, the $S = {}^1/_2$ metal electron is symmetrically delocalized between the two rhodium atoms, which now should exhibit quite equivalent anisotropic magnetic couplings.

As a summary, Table 5 compiles the X-band EPR parameters of complexes **5**−**7** under different experimental conditions. As previously pointed out, complexes **6** and **7** display a spectral behavior similar to that **5**, even if a more consistent radical-type paramagnetism was evident for **7** in the solid state as well as in solution. This spectral behavior points out that the nature of the axially bound radical significantly affects the paramagnetic features of the present complexes. Both of the $[TCQM]^{\bullet-}$ and $[2,5\text{-DMDCNQI}]^{\bullet-}$ subunits display relatively broad but well-resolved fluid solution hpf structures. The former exhibits 13 lines, with respect to 25 theoretically expected; the latter gives rise to 23 lines, with respect to 75 theoretically expected, likely as a consequence of metal-induced line-broadening effects. Finally, as expected, complex **5A** only exhibits the metal-in absorption of the $[Rh_2(form)_4]^{\bullet+}$ paramagnetic fragment.

Conclusions

Complex **I** reacts with polycyano ligands by simple axial coordination, while complex **II** reacts by accomplishing both coordination and redox processes. The different redox aptitude of the two complexes, reflected by their Rh(II)−Rh(II)/Rh(II)−Rh(III) oxidation potentials (for instance in MeCN solution: 0.53 V *vs* 0.00V), may reasonably account for the different behavior of the two species. We have also reported the unprecedented transformation of the $[C_2(CN)_4]^{\bullet-}$ radical anion into the tricyanomethanide ion, which coordinates to the $[Rh_2(form)_4]^{\bullet+}$ cation leading to the formation of a new example of a tricyanomethanide complex.

Acknowledgment. Financial support from MURST and Italian CNR is gratefully acknowledged. We are indebted to Dr A. Ceccanti for his help in the electrochemical measurements.

Supporting Information Available: Tables S1−S6, giving details of crystallographic data and structure refinement, anisotropic thermal parameters, hydrogen atom coordinates, full listing of bond lengths and angles (8 pages). Ordering information is given on any current masthead page.

IC9603868

(41) Phillips, W. D.; Rowell, J. C.; Weissman, S. I. *J. Chem. Phys.* **1960**, *33*, 626.